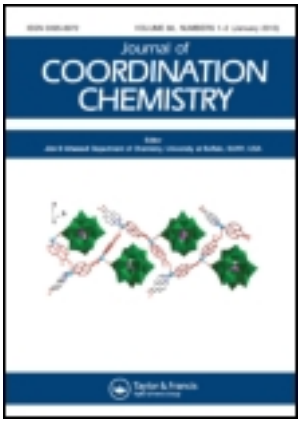

Journal of Coordination Chemistry
Publication details, including instructions for authors and subscription information:
http://www.tandfonline.com/loi/gcoo20

Five complexes containing N,N-bis(2-hydroxyethyl)-ethylenediamine with tetracyanidopalladate(II): synthesis, crystal structures, thermal, magnetic, and catalytic properties

Ş. Aslan Korkmaz [a], A. Karadağ [b], N. Korkmaz [b], Ö. Andaç [c], N. Gürbüz [d], İ. Özdemir [d] & R. Topkaya [e]

[a] Aquaculture Department, Vocational College, Tunceli University, Tunceli, Turkey

[b] Chemistry Department, Gaziosmanpaşa University, Tokat, Turkey

[c] Chemistry Department, Ondokuz Mayıs University, Samsun, Turkey

[d] Chemistry Department, İnönü University, Malatya, Turkey

[e] Physics Department, Gebze Institute of Technology, Kocaeli, Turkey

Accepted author version posted online: 01 Jul 2013.Published online: 14 Aug 2013.

To cite this article: Ş. Aslan Korkmaz, A. Karadağ, N. Korkmaz, Ö. Andaç, N. Gürbüz, İ. Özdemir & R. Topkaya (2013) Five complexes containing N,N-bis(2-hydroxyethyl)-ethylenediamine with tetracyanidopalladate(II): synthesis, crystal structures, thermal, magnetic, and catalytic properties, Journal of Coordination Chemistry, 66:17, 3072-3091, DOI: 10.1080/00958972.2013.820827

To link to this article: http://dx.doi.org/10.1080/00958972.2013.820827

Journal of Coordination Chemistry, 2013
Vol. 66, No. 17, 3072–3091, http://dx.doi.org/10.1080/00958972.2013.820827

Five complexes containing *N*,*N*-bis(2-hydroxyethyl)-ethylenediamine with tetracyanidopalladate(II): synthesis, crystal structures, thermal, magnetic, and catalytic properties

Ş. ASLAN KORKMAZ†, A. KARADAĞ*‡, N. KORKMAZ‡, Ö. ANDAÇ§
N. GÜRBÜZ¶, İ. ÖZDEMIR¶ and R. TOPKAYA‖

†Aquaculture Department, Vocational College, Tunceli University, Tunceli, Turkey
‡Chemistry Department, Gaziosmanpaşa University, Tokat, Turkey
§Chemistry Department, Ondokuz Mayıs University, Samsun, Turkey
¶Chemistry Department, İnönü University, Malatya, Turkey
‖Physics Department, Gebze Institute of Technology, Kocaeli, Turkey

(*Received 4 March 2013; in final form 6 June 2013*)

Five cyanide complexes, [Ni(*N-bishydeten*)Pd(CN)$_4$] (**1**), [Cu(*N-bishydeten*)Pd(μ-CN)$_2$(CN)$_2$]$_n$ (**2**), [Cu(*N-bishydeten*)$_2$][Pd(CN)$_4$] (**3**), [Zn(*N-bishydeten*)Pd(CN)$_4$] (**4**), and [Cd(*N-bishydeten*)$_2$][Pd(CN)$_4$] (**5**) (*N-bishydeten* = *N*,*N*-bis(2-hydroxyethyl)-ethylenediamine), have been synthesized and characterized using various techniques. Different structures were formed when the M : L ratio was varied in copper complexes. The single-crystal X-ray diffraction analysis reveals that **2**, a 1-D cyanide-bridged complex with 2,2-*CT*-type *zigzag* chain, was obtained by using 1 : 1 M : L ratio whereas **3** was formed as a complex salt in a molar ratio of 1 : 2. The thermal stabilities determined from DTG_{max} values of the first decomposition stages change in the order **1** > **5** > **4** > **3** > **2**. Although an EPR signal was not observed for **1**, the *g* parameters obtained from the EPR spectra of **2** and **3** indicate that Cu^{II} ions are located in tetragonally distorted octahedral sites (D_{4h}), and the ground state of the unpaired electron is $d_{x^2-y^2}$ ($^2B_{1g}$). The magnetic behavior indicates a very small antiferromagnetic interaction below 10 K for **1–3**. In **3**, there is a temperature-independent paramagnetism (α) due to the orbital moments of the *d* electrons. **1–3** were tested as catalysts in Suzuki and Heck coupling reactions.

Keywords: Tetracyanidopalladate; *N*,*N*-bis(2-hydroxyethyl)-ethylenediamine; Thermal analysis; Magnetic susceptibility; Suzuki–Heck coupling reaction

1. Introduction

The wide availability of transition metal cyanide complexes in terms of both diverse bonding and structural chemistry has led to widespread application of these complexes in materials chemistry. Cyanide is an efficient ligand for stabilization and the formation of one- (1-D), two- (2-D), or three-dimensional (3-D) structures. The versatility of cyanide results from its ability to act as both a σ-donor and a π-acceptor, its negative charge, and its ambidentate nature [1]. A terminal cyanide can participate in simple hydrogen bonds of

*Corresponding author. Email: ahmet.karadag@gop.edu.tr

the CN···H−X type (X is an electronegative atom). These hydrogen bonds play an important role in forming high-dimensional structures, packing and stabilizing the structures formed, and serving as a possible exchange path for magnetic interactions [2]. Cyanide has been widely used in luminescence [3, 4], catalysis [5, 6], molecular sieves [7–10], ion exchange [11], selective binding of guest molecules [12–14], and magnetism [15–20].

The controlled assembly of inorganic building blocks is very important in design of high-dimensional systems. These systems are formed using $[M(CN)_n]^{y-}$ (M = Ni, Pd, Pt, Cu and Au; n = 2 or 4; $y = -1$ or -2) in conjunction with a transition metal complex because of the ability of cyanide to connect various central atoms to build molecular assemblies [21]. Among these cyanidometallates, the tetracyanidopalladate, $[Pd(CN)_4]^{2-}$, is an ideal building block that has rarely been studied. Square planar Pd^{II} units have attracted attention as catalysts in C–C coupling reactions. Palladium-catalyzed C–C cross-coupling reactions, such as the Suzuki–Miyaura [22–29] and the Heck–Mizoroki [30–34], are among the most essential transformations in organic and organometallic chemistry.

Functional cyanide complexes can be synthesized with di- or poly-dentate ligands [35]. The tripodal *N-bishydeten* used in this study is a neutral ligand that has two *N*- and two *O*-donors, and behaves as a multidentate ligand, generally coordinated with *NN′O* or *NN′* O_2 donors [36, 37]. It has rarely been used in cyanide complexes.

We reported a number of cyanidometallate complexes in which $[Pd(CN)_4]^{2-}$ has been utilized. Previous studies on structures of 1-D bimetallic polymeric cyanide complexes $[M(hydeten)_2Pd(CN)_4]_n$ {M^{II} = Ni, Cu, Zn and Cd; *hydeten* = *N*-(2-hydroxyethyl-ethylenediamine)} [38–40] revealed that Cu/Pd and Zn/Pd binuclear complexes, having 2,2-*TT*-type chains, were isostructural whereas Cd/Pd complexes formed in 2,2-*CT*-type chains. The cyanide-bridged complexes $[M(bishydeten)Pd(CN)_4]$ {M^{II} = Ni, Cu, Zn and Cd; *bishydeten* = *N*,*N′*-bis(2-hydroxyethyl)-ethylenediamine} were synthesized and characterized, and the catalytic properties of Ni/Pd and Cu/Pd complexes were studied [41]. As an extension of our work on these systems, here we report the synthesis and characterization (FT-IR spectra, elemental analysis, EPR spectra, and thermal properties) of **1–5**. The crystal structures of **2** and **3,** and the magnetic behavior and catalytic properties of **1–3** were also determined.

2. Experimental

2.1. *Materials and instrumentation*

High purity $PdCl_2$ (Alfa Aesar), $NiCl_2·6H_2O$ (Surchem), $CuCl_2·2H_2O$ (Merck), $ZnCl_2$ (Panreac), $CdSO_4·8/3H_2O$ (Sigma), KCN (Merck), and *N*,*N*-bis(2-hydroxyethyl)-ethylenediamine ($C_6H_{16}N_2O_2$) (Aldrich) were used as received.

Elemental analyses for C, H, and N were carried out by standard methods using a CHNS-932 (LECO) Elemental Analyzer at the Middle East Technical University and İnönü University. IR spectra were recorded on a Jasco 430 FT-IR spectrophotometer with KBr pellets from 4000 to 400 cm^{-1} (Gaziosmanpaşa University, TURKEY). Perkin–Elmer PYRIS Diamond TG/DTA thermal analyzer was used to record simultaneous TG, DTG, and DTA curves under nitrogen at a heating rate of 10 °C min^{-1} from 35 to 1350 °C using platinum crucibles (Gaziosmanpaşa University, TURKEY). The EPR powder spectrum was

recorded with a Bruker EMX X-band spectrometer (9.8 GHz) with about 20 mW microwave power and 5 kHz magnetic field modulation. The 10–300 K magnetization measurements were carried out on a Quantum Design PPMS system. The χ–T graphs were recorded under constant magnetic fields of 0.5 kOe and 5 kOe (Gebze Institute of Technology, TURKEY). Concurrently, all reactions were monitored on an Agilent 6890 N GC system by GC-FID with a HP-5 column of 30 m length, 0.32 mm diameter, and 0.25 μm film thicknesses for catalysis. Column chromatography was performed by using silica gel 60 (70–230 mesh) (solvent ratios are given as v/v) (İnönü University, TURKEY).

2.2. *Synthesis*

2.2.1. [Ni(N-bishydeten)Pd(CN)$_4$] (1). Solid KCN (4 mM) and $NiCl_2 \cdot 6H_2O$ (1 mM) were added to a water-ethanol solution (1 : 1; 20 mL) of $PdCl_2$ (1 mM). To the resulting light blue mixture, an ethanolic solution (15 mL) of *N*,*N*-bis(2-hydroxyethyl)-ethylenediamine (*N-bishydeten*) (1 mM) was added dropwise and the reaction mixture was stirred for 45 min. The lilac precipitate formed was filtered, washed with water and ethanol, and dried in air. Yield: 60%. Elemental analyses (C, H, and N) were carried out. Anal. Calcd for **1** {$C_{10}H_{16}N_6O_2NiPd$ (417.39)} (%): C, 28.78; H, 3.86; N, 20.13. Found: C, 28.63; H, 3.93; N, 19.63. Infrared spectra exhibited the following absorptions: 3602, 3310 (ν_{OH}); 3195 (ν_{NH}); 2979, 2910, 2862 (ν_{CH}); 2178, 2145 ($\nu_{C\equiv N}$); 1621 (δ_{NH}); 1462 (δCH_2); 1113 (ν_{CN}); 1023 (ν_{CO}).

2.2.2. [Cu(N-bishydeten)Pd(μ-CN)$_2$(CN)$_2$]$_n$ (2). KCN (4 mM) was added to a water–ethanol solution (1 : 1; 20 mL) of $PdCl_2$ (1 mM) and $CuCl_2 \cdot 2H_2O$ (1 mM) was added to the resulting colorless clear solution. An ethanolic solution (15 mL) of *N-bishydeten* (1 mM) was then slowly added to the green cloudy mixture. A brilliant blue solution formed, was stirred for an hour and then filtered. After a few weeks, shiny deep blue single crystals were obtained for X-ray analysis by slow evaporation at room temperature. Yield: 37%. Elemental analyses (C, H, and N) were carried out. Anal. Calcd for **2** {$C_{10}H_{16}N_6O_2CuPd$ (422.24)} (%): C, 28.45; H, 3.82; N, 19.90. Found: C, 28.45; H, 3.78; N, 19.30. Infrared spectra exhibited the following absorptions: 3490 (ν_{OH}); 3264, 3232, 3147 (ν_{NH}); 2985, 2952, 2885, 2835 (ν_{CH}); 2187, 2143 ($\nu_{C\equiv N}$); 1598 (δ_{NH}); 1455 (δCH_2); 1130 (ν_{CN}); 1060 (ν_{CO}).

2.2.3. [Cu(N-bishydeten)$_2$][Pd(CN)$_4$] (3). The synthesis of **3** was carried out using the same procedure as described for **2**, but this time 2 mM *N-bishydeten* was added, yielding prism-shaped dark violet single crystals by slow evaporation. Yield: 37%. Elemental analyses (C, H, and N) were carried out. Anal. Calcd for **3** {$C_{16}H_{32}N_8O_4CuPd$ (570.44)} (%): C, 33.69; H, 5.65; N, 19.64. Found: C, 33.94; H, 5.61; N, 19.71. Infrared spectra exhibited the following absorptions: 3385, 3289 (ν_{OH}); 3229, 3151 (ν_{NH}); 2979, 2949, 2889 (ν_{CH}); 2127 ($\nu_{C\equiv N}$); 1595 (δ_{NH}); 1471 (δCH_2); 1152 (ν_{CN}); 1083, 1059 (ν_{CO}).

2.2.4. [Zn(N-bishydeten)Pd(CN)$_4$] (4). **4** was synthesized by the procedure adopted for **1** using $ZnCl_2$ instead of $NiCl_2 \cdot 6H_2O$. Yield: 31%. Elemental analyses (C, H, and N) were

carried out. Anal. Calcd for **4** {$C_{10}H_{16}N_6O_2ZnPd$ (424.08)} (%): C, 28.32; H, 3.80; N, 19.82. Found: C, 28.83; H, 4.00; N, 19.37. Infrared spectra exhibited the following absorptions: 3316 (ν_{OH}); 3271, 3142 (ν_{NH}); 2967, 2922, 2871, 2838 (ν_{CH}); 2164, 2137 ($\nu_{C\equiv N}$); 1585 (δ_{NH}); 1474 (δCH_2); 1161 (ν_{CN}); 1070, 1016 (ν_{CO}).

2.2.5. [Cd(N-bishydeten)$_2$][Pd(CN)$_4$] (5). **5** was synthesized by the procedure adopted for **3** using $CdSO_4 \cdot 8/3H_2O$ instead of $CuCl_2 \cdot 2H_2O$. Yield: 44%. Elemental analyses (C, H, and N) were carried out. Anal. Calcd for **5** {$C_{10}H_{16}N_6O_2CdPd$ (619.31)} (%): C, 31.03; H, 5.21; N, 18.09. Found: C, 31.31; H, 5.21; N, 18.28. Infrared spectra exhibited the following absorptions: 3353 (ν_{OH}); 3353, 3292 (ν_{NH}); 2970, 2883, 2829 (ν_{CH}); 2141, 2129 ($\nu_{C\equiv N}$); 1595 (δ_{NH}); 1450 (δCH_2); 1146 (ν_{CN}); 1079 (ν_{CO}).

2.3. *Catalysis studies*

2.3.1. General procedure for the Heck coupling reaction. **1** (1.0%, molar ratio), aryl bromide (1.0 mM), styrene (1.5 mM), Cs_2CO_3 (2 mM), and DMF (3 mL) were added to a small Schlenk tube in air and the mixture was heated at 80 °C for 6 h. When the reaction was completed, the mixture was cooled, extracted with ethyl acetate/hexane (1 : 5), and filtered through a pad of silica gel with copious washing, and then concentrated and purified using flash chromatography on silica gel. The same procedure was performed for **2** and **3** using K_2CO_3 instead of Cs_2CO_3, and the reaction mixtures were heated for 15 h. The purity of the compounds was checked by NMR and GC, and the yields were based on aryl bromide. All reactions were monitored by GC-FID with an HP-5 column of 30 m length, 0.32 mm diameter, and 0.25 μm film thicknesses.

2.3.2. General procedure for the Suzuki coupling reaction. **1** (1.0 mM%), aryl bromide (1.0 mM), phenylboronic acid (1.5 mM), Cs_2CO_3 (2 mM), and dioxane (3 mL) were added to a small Schlenk tube in air and the mixture was heated at 80 °C for 6 h. At completion of the reaction, the mixture was cooled, extracted with ethyl acetate/hexane (1 : 5), filtered through a pad of silica gel with copious washings, concentrated, and purified using flash chromatography on silica gel. The same procedure was performed for **2** and **3** using K_2CO_3 instead of Cs_2CO_3, and the reaction mixtures were heated for 15 h. The purity of the compounds was checked by NMR and GC, and yields are based on aryl bromide.

2.4. *Crystallographic data collection and structure refinement*

Of the synthesized complexes, **2** and **3** were obtained as single crystals for X-ray analysis.

Single crystal X-ray diffraction intensities of **2** were collected at room temperature using a four-circle Rigaku R-AXIS RAPID-S diffractometer with a 2-D IP area detector at room temperature. Graphite-monochromated MoKα radiation ($\lambda = 0.71073$ Å) and oscillation scan techniques ($\Delta\omega = 5°$ for one image) were used for data collection. The lattice parameters were determined by least-squares on the basis of all reflections with $F^2 > 2\sigma(F^2)$. The intensity integrations, correction for Lorentz and polarization effects, and cell refinement were performed using Crystal-Clear software [42].

Intensity measurements of **3** were made at room temperature on a STOE IPDS 2 image plate detector system using graphite monochromated MoKα radiation ($\lambda = 0.71073$ Å). STOE X-AREA [44] was used for data collection and cell refinement, and STOE X-RED [45] was used for data reduction.

The structures were solved by direct methods using SHELXS-97 [43] and nonH atoms were refined using full-matrix least-squares with anisotropic temperature factors (SHEL-XL-97) [43]. Calculated positive residual density and deepest hole around Pd are observed in both structures.

C7 of *N-bishydeten* in **2** are disordered about a mirror plane which bisects C6, N4, N5, Cu1, N2, C2, Pd1, C3 and N3. Due to the disorder of C7, the positions of hydrogens attached to N5 and C6 were also disordered.

Uncoordinated hydroxyl oxygen (O2a, O2b) of *N-bishydeten* in **3** is positionally disordered over two position with a ratio of 0.75(1)/0.25(1). Similarity restraints SAME, SIMU, and DELU were applied to disordered oxygen.

Molecular graphics were obtained using ORTEP-3 [45] for Windows; DIAMOND [46] and material for publication was prepared using WinGX [47] programs. Crystallographic data for **2** and **3** are reported in table 1.

CCDC ID 881936 and CCDC ID 840626 contain the crystallographic data for **2** and **3**, respectively. These data can be obtained free charge of via https://www.ccdc.cam.ac.uk/

Table 1. Crystal data and structure refinement parameters for **2** and **3**.

	2	**3**
Empirical formula	$C_{10}H_{16}N_6O_2CuPd$	$C_{16}H_{32}N_8O_4CuPd$
Formula weight	422.23	570.44
$F(000)$	836	582
Temperature [K]	293(2)	293(2)
Crystal size [mm]	$0.23 \times 0.14 \times 0.10$	$0.41 \times 0.35 \times 0.27$
Crystal system	Orthorhombic	Monoclinic
Space group	*Pnma*	$P2_1/c$
a [Å]	14.9784(2)	10.2975(19)
b [Å]	11.8554(2)	7.4922(11)
c [Å]	8.5875(2)	16.813(3)
α [°]	90	90
β [°]	90	121.211(12)
γ [°]	90	90
V [Å^3]/Z	1524.92(5)/4	1109.4(3)/2
D_{Calcd} [g/cm^3]	1.839	1.708
μ [mm^{-1}]	2.583	1.808
θ range [°]	2.72–26.41	2.31 – 27.55
Index ranges	$-18 \leqslant h \leqslant 18$, $-14 \leqslant k \leqslant 13$, $-10 \leqslant l \leqslant 10$	$-13 \leqslant h \leqslant 13$, $-9 \leqslant k \leqslant 9$, $-21 \leqslant l \leqslant 21$
Reflections collected	31,528	7844
Reflections observed	1503	1928
Data/restraints/parameters	1639/0/109	2559/6/149
R_1/wR_2	0.0324/0.0775	0.0462/0.1135
GooF	1.12	1.074
Absorption correction	Multi-scan	Integration
w	$1/[\sigma^2(F_0^2)+(0.0278P)^2+0.0843P]$ $P = (F_0^2 + 2F_c^2)/3$	$1/[\sigma^2(F_0^2)+(0.0604P)^2+0.7275P]$ $P = (F_0^2 + 2F_c^2)/3$
S, $(\Delta/\sigma)_{max}$	1.12/0.001	1.073/0.000
$\Delta\rho_{max}$, $\Delta\rho_{min}$ (eÅ^{-3})	0.359/−0.839	0.951/−1.815

$R_1 = \sum ||F_0| - |F_c|| / \sum |F_0|, wR_2 = \left\{ \sum \left[w(F_0^2 - F_c^2)^2 \right] / \sum \left[w(F_0^2)^2 \right] \right\}^{1/2}$.

services/structure_deposit/ or from the Cambridge Crystallographic Data Center, 12 Union Road, Cambridge CB2 1EZ, UK; Fax: (+44) 1223-336-033 or E-mail: deposit@ccdc.cam.ac.uk.

3. Results and discussion

3.1. *FT-IR spectra*

In the FT-IR spectrum of *N-bishydeten*, absorption bands arising from υOH and υNH_2, υCH_2, δNH_2, δCH_2, υC–N, and υCO are observed at 3400–3250, 2948–2832, 1570, 1471, 1148, and 1036 cm^{-1}, respectively [36]. The FT-IR spectra of **1–5** exhibit absorptions that confirm the presence of all functional groups of *N-bishydeten*, which coordinates via its NH_2 and OH.

The characteristic feature in spectra of metal complexes that contain cyanide are sharp and strong bands between 2000 and 2200 cm^{-1} resulting from υ(C≡N). The number and positions of υ(C≡N) absorptions reveal bridging or terminal cyanide in the complexes. Cyanide stretches of ionic cyanides such as NaCN and KCN are observed at 2080 cm^{-1}, and this peak shifts to 2143 cm^{-1} in $[Pd(CN)_4]^{2-}$ because of coordination of cyanide to palladium as a terminal ligand. As a result of bridging cyanide (Pd–CN–M′), the cyanide stretch is above 2143 cm^{-1}. Splitting of cyanide stretch is evidence of the existence of bridging and terminal cyanide [48]. IR spectra of **1** and **4** exhibit two sharp bands (2178 and 2145 cm^{-1} for **1** and 2164 and 2137 cm^{-1} for **4**) that are attributed to the presence of both bridged and terminal CN^-; the lower wavenumber corresponds to a nonbridging cyanide and the higher wavenumber corresponds to a bridging cyanide. The intensity of the lower wavenumber is stronger than that of the higher wavenumber. Such shifts have been observed in cyanide-bridged complexes such as $[Zn(hydeten)_2Pd(CN)_4]$ and $[Cd(hydeten)_2Pd(CN)_4]$ [39], $[M(bishydeten)Pd(CN)_4]$ (M^{II} = Ni,Cu and Zn) [41], $[Cu(dpt)Pd(CN)_4]$ (*dpt* = 3,3'-iminobispropylamine) [49], $[Ni(edbea)Pd(CN)_4]$, and $[Zn_2(edbea)_2Pd(CN)_4]$ (*edbea* = 2,2'-(ethylenedioxy)bis(ethylamine)) [50].

Descriptions of the spectra of **2** and **3** are more useful when the crystal structures of the complexes are known. The spectrum of **2** exhibits a split band at 2187 and 2143 cm^{-1}, indicating bridging and terminal cyanide. These data were confirmed by the X-ray analysis that **2** is a polymeric substance of the form $[Cu(N\text{-}bishydeten)Pd(CN)_4]_n$. **3** has only one absorption at 2127 cm^{-1} from terminal cyanide in the anion. This result was confirmed by the X-ray analysis. This has also been observed in $[Cu(edbea)_2Pd(CN)_4]$ and $[Cd(edbea)_2][Pd(CN)_4]$ [50]. In **5**, the CN^- stretches at 2127 and 2141 cm^{-1} correspond to nonequivalent terminal CN^-. The lower wavenumber is attributed to the isolated $[Pd(CN)_4]^{2-}$; the band at 2141 cm^{-1} is attributed to a pair of terminal cyanides involved in different hydrogen bonding.

3.2. *X-ray single crystal analysis*

Notably, varying the M (metal) : L (ligand) ratio results in formation of different structures. **2** has a composition of $[Cu(N\text{-}bishydeten)Pd(CN)_4]$ (**2**) with a molar ratio 1 : 1 and **3** has a composition of $[Cu(N\text{-}bishydeten)_2][Pd(CN)_4]$ (**3**) with a molar ratio 1 : 2.

3.2.1. Crystal structure of {catena-poly[[dicyanido-1κ^{2}C-μ-cyanido-1 : 2κ^{2}C:N-[N,N-bis(2-hydroxyethyl)-ethylenediamine-2κ^{4}N,N',O,O']copper(II)palladium(II)]-μ-cyanido-1 : 2'κ^2 C:N]},[Cu(N-bishydeten)(μ-CN)$_2$(CN)$_2$]$_n$ (2). The crystal structure of **2** depicts a 1-D cyanide-bridged polymeric *zigzag* chain which is isostructural with [Zn(*hydeten*)$_2$Pt(CN)$_4$] [35] and [Cd(*hydeten*)$_2$Pd(CN)$_4$] [39] (figure 1(a)). Bridging cyanide groups are *cis* in the cationic segment whereas these groups occupy *trans* positions in the anionic part. Therefore, the chain of **2** can be classified as a 2,2-*CT*-type chain. There are only a few examples of Pd-containing cyanide-bridged complexes exhibiting *zigzag* chain structures with a 2,2-*CT*-type chain [39] (figure 1(b)).

Heterometallic assembly is formed by achiral [Cu(*N-bishydeten*)]$^{2+}$ and square-planar [Pd(CN)$_4$]$^{2-}$ building blocks connected by μ–CN$^-$. *N-bishydeten* is bulky and tetradentate in this compound. Thus, it surrounds Cu. The *cis* positions in the equatorial plane of Cu^{II} are occupied by nitrogens of the bridging cyanide. Cu1 coordination sphere exhibits distorted octahedral geometry with four donors from one *N-bishydeten* (N4, N5, O1 and O1^i) and two from different tetracyanidopalladates (N2 and N3^{ii}) (symmetry codes: (i) $x-2$, $-y-3/2$, $z-2$; (ii) $x-1/2$, y, $-z-3/2$). Extremely long axial semi-coordination Cu1-O1 bonds of **2** are observed. In accord with the pseudo Jahn–Teller effect, axial

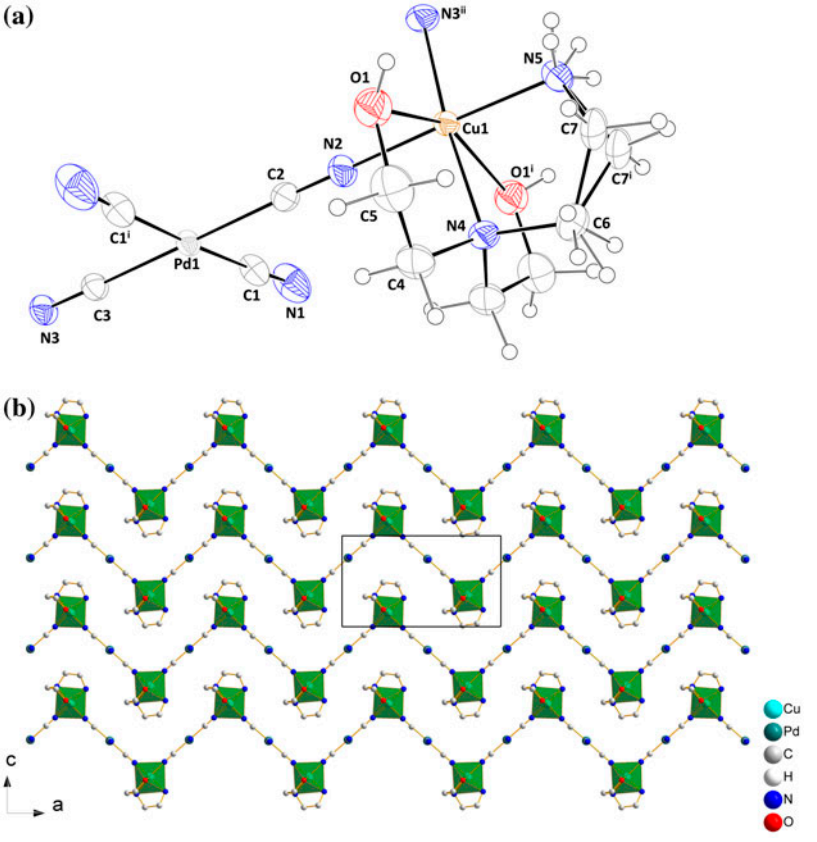

Figure 1. (a) The molecular structure of polymeric **2**, with the atom-numbering scheme, and (b) the *zigzag* chain of polymeric structure of **2** (symmetry codes: (i) $x-2$, $-y-3/2$, $z-2$; (ii) $x-1/2$, y, $-z-3/2$).

Cu1–O1 bond distances are longer than equatorial bond distances (Cu1–N2, Cu1–N3^{ii}, Cu1–N4, and Cu1–N5), as shown in table 2. The bond observed between tertiary amine nitrogen and Cu^{II} (Cu1–N4: 2.066(3) Å) is longer than that of the primary amine nitrogen (Cu1–N5: 1.997(4) Å), from different steric environments of the amines. Bond lengths in the coordination environment of the Cu^{II} ion follow the order O1 > N4 > N5 > N2 > N3^{ii}. The Cu1–N bond distances in **2** are similar to those of other Cu^{II} complexes of this type [36, 38, 39, 41, 49–56]. The N–Cu1–N bond angles deviate from ideal values (84.6(15)° and 178.4(16)°), attributed to steric effects arising from the shape of the ligand. The crystal packing of **2** is shown in figure 2.

Each Pd^{II} is coordinated by four cyanides in a square planar geometry, and the Pd1–C and C≡N bond lengths are 1.984(4)–2.001(4) Å and 1.130(6)–1.142(5) Å, respectively. These data are within the range of typical values for cyanide-bridged complexes containing tetracyanidopalladate [38, 39, 49–54, 57–59]. However, a slight bending occurs at N-C-Pd angles. There are two terminal and two bridged cyanides in $[Pd(CN)_4]^{2-}$, and the bridging Pd1–C2 and Pd1–C3 bond distances (1.990(4) and 2.001(4) Å) are longer than the Pd1–C1 (1.984(4) Å) bond distance. All nitrogens of terminal $[Pd(CN)_4]^{2-}$ moieties in **2** are involved in intermolecular N-H···N and O–H···N hydrogen bonds (figure 3).

In N-H···N weak hydrogen bonds, the upper limit for the N···N distance is 3.38 Å [51]. In **2**, N5···N1 interactions involving H5C and H5D, respectively, are shorter than 3.38 Å (table 3).

3.2.2. Crystal structure of [Cu(N-bishydeten)$_2$][Pd(CN)$_4$] (3). Single crystal X-ray analysis reveals that **3** is an ionic complex salt, isostructural with [Cu(*N-bishydeten*)$_2$][Ni(CN)$_4$] [36] and [Ni(*N-bishydeten*)$_2$][Pt(CN)$_4$] [60]. This type of structure can be typically seen in the literature [61–65]. In **3**, *N-bishydeten* serves as a tridentate ligand with *N,N′,O*

Table 2. Selected bond distances and angles of **2**.

Bond lengths (Å)			
Cu1–N2	1.977(4)	Pd1–C1	1.984(4)
Cu1–N3	1.973(3)	Pd1–C2	1.990(4)
Cu1–N4	2.066(3)	Pd1–C3	2.001(4)
Cu1–N5	1.997(4)	C1–N1	1.142(5)
Cu1–O1	2.449(3)	C2–N2	1.130(6)
		C3–N3	1.131(5)
Bond angles (°)			
N2–Cu1–N5	178.4(16)	C1^{i}–Pd1–C1	177.3(18)
N3^{ii}–Cu1–N4	174.5(15)	C1–Pd1–C2	88.7(9)
O1–Cu1–O1^{i}	154.0(9)	C1–Pd1–C3	91.2(9)
N3^{ii}–Cu1–N2	91.7(17)	C2–Pd1–C3	179.7(16)
N2–Cu1–O1	87.0(15)	N1–C1–Pd1	177.5(3)
N5–Cu1–N4	84.6(15)	N2–C2–Pd1	178.9(4)
N3^{ii}–Cu1–N5	89.9(16)	N3–C3–Pd1	179.1(4)
N2–Cu1–N4	93.8(15)	C2–N2–Cu1	179.8(4)
N4–Cu1–O1	77.6(15)	C3–N3^{ii}–Cu1	176.5(4)
N5–Cu1–O1	92.7(15)	C6–N4–Cu1	108.7(3)
N3–Cu1–O1	102.7(15)	C4–N4–Cu1	108.1(2)
		C7–N5–Cu1	109.7(3)

Symmetry codes: (i) $x-2$, $-y-3/2$, $z-2$; (ii) $x-1/2$, y, $-z-3/2$.

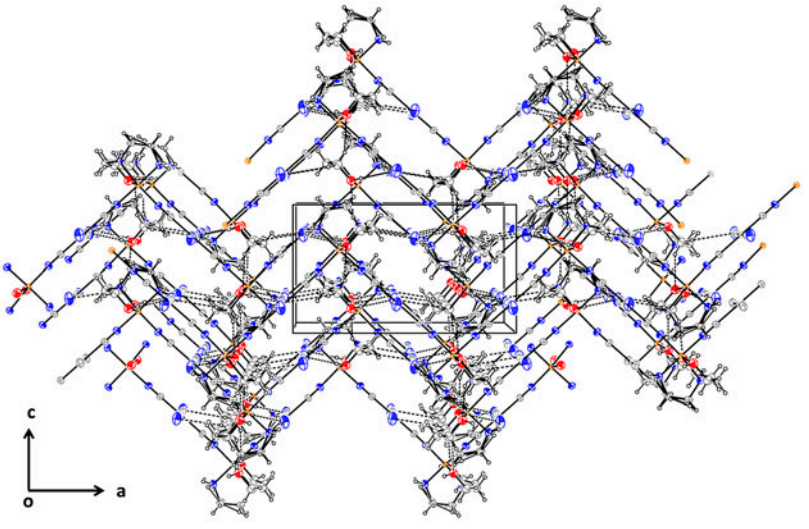

Figure 2. The crystal packing of **2**.

donors. The complex salt consists of $[Cu(N\text{-}bishydeten)_2]^{2+}$ and $[Pd(CN)_4]^{2-}$, and the atom labeling scheme is shown in figure 4.

In the structure of **3**, Cu^{II} and Pd^{II} both occupy sites of inversion centers. The Cu^{II} is six-coordinate with four nitrogens (N1, N2, $N1^{ii}$ and $N2^{ii}$) in the equatorial plane and two oxygens (O1 and $O1^{ii}$) in the axial positions provided by the two tridentate *N-bishydeten* ligands (symmetry code: (ii) $1-x$, $1-y$, $1-z$). The Cu1–N1 (2.004(3) Å) bond with the nitrogen of primary amine is shorter than Cu1–N2 (2.103(3) Å) with the nitrogen belonging to the tertiary one. This difference may be a result of steric hindrance from the noncoordinating ethanol edge of the *N-bishydeten* ligand (table 4). A d^9 system forms slightly distorted and tetragonally elongated octahedral coordination. Therefore, these Cu–N distances are significantly shorter than observed for Cu–O1 (2.401(2) Å). The Cu–N bond distances in **3** are similar to those of other Cu^{II} complexes of this type [36, 38, 40, 41, 49–56].

The diamagnetic $[Pd(CN)_4]^{2-}$ (figure 5) has Pd1-C bond distances identical (within 3σ), with an average value of 1.998 Å. Like Cu^{II}, Pd^{II} in the inversion center forms linear bond angles with cyanido carbons. The C≡N bonds (1.145(4) and 1.152(5) Å), and the Pd1–C≡N angles (177.6(3) and 177.3(3)°) are in accord with other tetracyanidopalladates [40, 41, 52–54, 57–59] (table 4).

The presence of nonbridging cyanide does not mean that cyanides are unimportant for stabilization of the crystal structure. In fact, these cyanides participate in a series of bifurcated hydrogen bonds with NH_2, CH_2, and OH of *N-bishydeten*. All hydrogen bonds have D···A distances ranging from 2.84(9) to 3.13(7) Å, and are effective in forming a layered structure (table 5, figure 6a and b).

3.3. *Thermal studies*

Thermal decomposition of cyanide complexes containing *N*-donor ligands is characterized by liberation of the *N*-donor ligands followed by decomposition of the cyanide groups, as

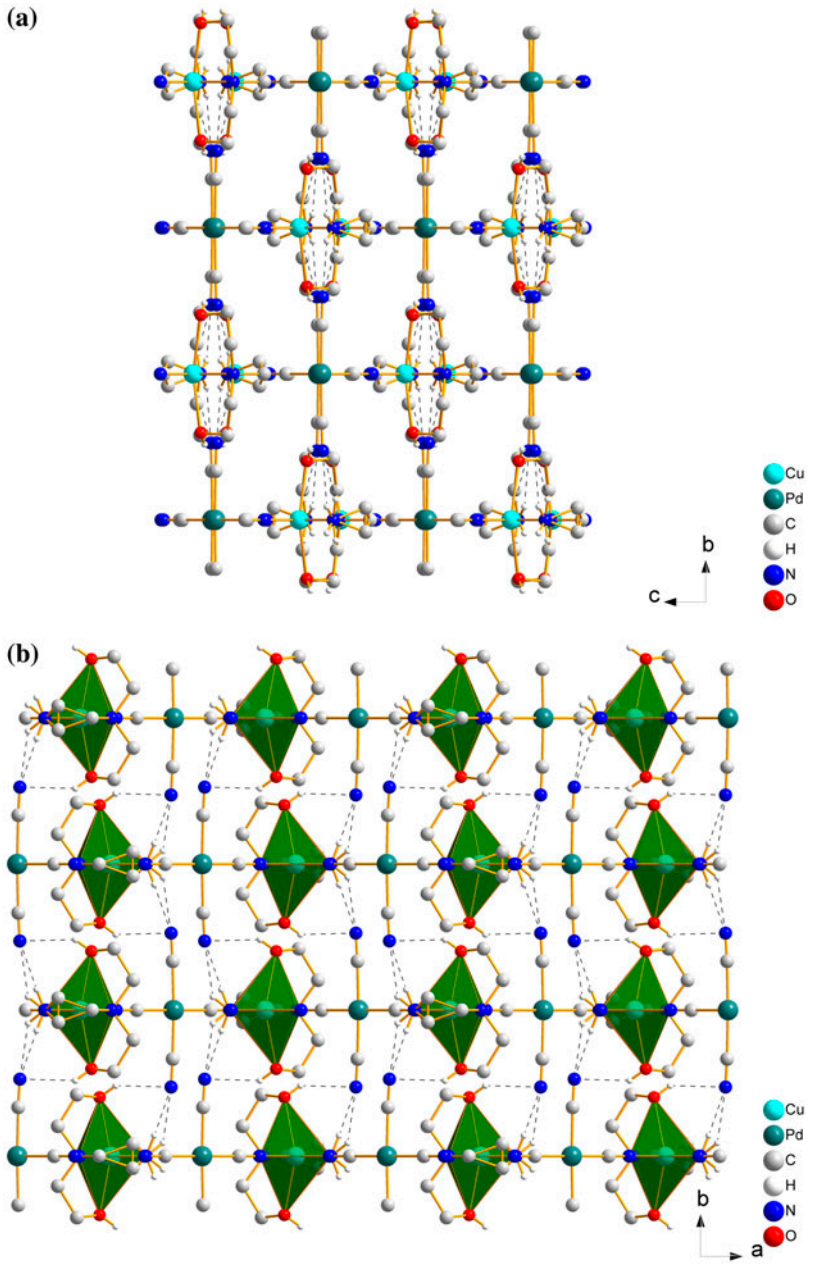

Figure 3. Hydrogen bonds of **2** formed by terminal cyanide along (a) the *a* axis and (b) the *c* axis.

observed in previous studies [66–70]. The thermal decomposition of **1–5** is consistent with this and has multi-step processes (Supplementary material). The DTA signal was automatically converted to a DSC signal and the enthalpy values (ΔH, J/g) of the decomposition steps were determined. The thermal analysis results are given in table 6.

Table 3. Hydrogen bonds of **2** (Å and °).

D–H···A	*d*(D–H)	*d*(H...A)	*d*(D...A)	∠ (DHA)
N5–H5C···N1^{i}	0.90	2.30	3.01(4)	135.73
N5–H5D···N1^{ii}	0.90	2.15	3.01(4)	158.96
O1–H1···N1^{ii}	0.82	2.30	2.99(4)	143.32

Symmetry codes: (i) $-x+1/2$, $-y$, $z+1/2$; (ii) $-x+1/2$, $y+1/2$, $z+1/2$.

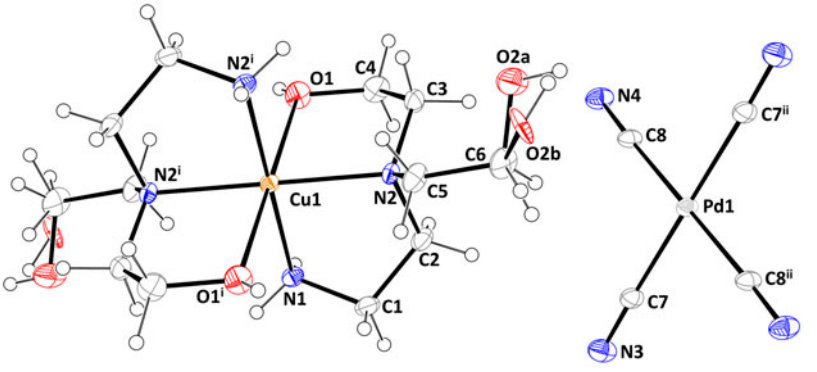

Figure 4. The molecular structure of **3** showing the atom numbering scheme (symmetry codes: (i) $-x$, $1-y$, $-z$; (ii) $1-x$, $1-y$, $1-z$).

Table 4. Selected bond distances and angles of **3**.

Bond lengths (Å)			
Cu1–N1	2.004(3)	Pd1–C8	1.997(3)
Cu1–N2	2.103(3)	Pd1–C7	1.996(4)
Cu1–O1	2.401(2)	C7–N3	1.145(4)
		C8–N4	1.152(5)
Bond angles (°)			
N1–Cu1–N1^{ii}	180.0	C2–N2–Cu1	107.0(2)
N2–Cu1–N2^{ii}	180.0(18)	N3–C7–Pd1	177.6(3)
O1–Cu1–O1^{ii}	180.0(16)	N4–C8–Pd1	177.3(3)
N1–Cu1–N2^{ii}	84.3(11)	C8–Pd1–C8^{i}	180.0(2)
N1–Cu1–N2	95.7(11)	C7–Pd1–C7^{i}	180.0(2)
N1–Cu1–O1^{ii}	97.2(10)	C8–Pd1–C7	92.5(12)
N1–Cu1–O1	82.8(10)	C8–Pd1–C7^{i}	87.5(12)
N2–Cu1–O1^{ii}	77.6(10)	C3–N2–Cu1	109.8(18)
N2–Cu1–O1	102.4(10)	C5–N2–Cu1	106.3(2)
C1–N1–Cu1	106.5(2)		

Symmetry codes: (i) $-x$, $1-y$, $-z$; (ii) $1-x$, $1-y$, $1-z$.

The thermal degradation of **1** is realized in two stages which can be distinguished clearly. The TG curve for **1** indicates that it is stable to 238 °C, at which decomposition begins. From 238 to 428 °C, weight loss of 48.40% corresponds to release of one *N-bishydeten* and two cyanides (Calcd 47.98%) by an endothermic process. In the second step, decomposition of the remaining two cyanides occurs from 438 to 733 °C with weight loss of 11.53% (Calcd 12.47%). The final product is a mixture of metallic Ni+Pd (solid residue 40.07%; Calcd 39.55%) for **1**.

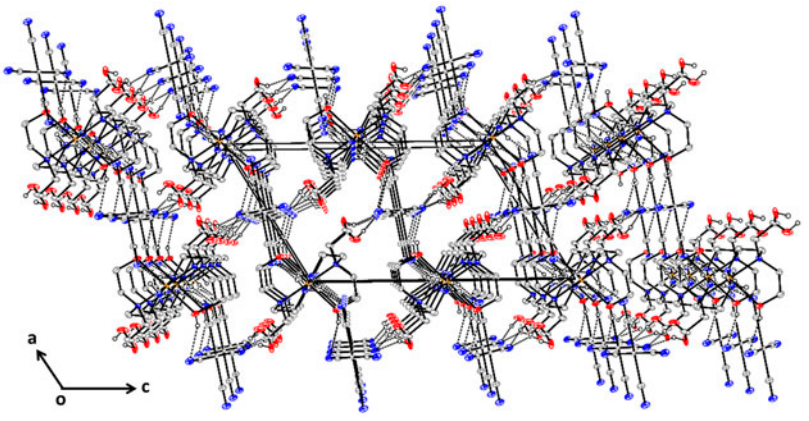

Figure 5. 3-D view of **3**. Hydrogens are omitted for clarity.

Table 5. Hydrogen bonds of **3** (Å and °).

D–H···A	*d*(D–H)	*d*(H...A)	*d*(D...A)	∠ (DHA)
N1–H1C···N4^{i}	0.90	2.29	3.13(7)	155.7
N1–H1D···N4^{ii}	0.90	2.17	3.05(7)	166.5
O1–H1···N3^{iii}	0.82	2.33	3.11(4)	158.0
O2A–H2C···N3^{iv}	0.82	2.10	2.86(5)	154.6
O2B–H2D···N3^{iv}	0.82	2.11	2.84(9)	148.9

Symmetry codes: (i) x, $5/2-y$, $1/2+z$; (ii) $-x$, $y+1/2$, $-z+1/2$; (iii) $x-1$, $5/2-y$, $1/2+z$; (iv) x, $-1+y$, z.

The thermal decomposition of **2** is similar to **1**, consisting of three stages. Two degradation steps at 145–206 °C and 206–438 °C with weight loss of 47.22% (Calcd 47.43%) correspond to release of one *N-bishydeten* and two cyanides (these steps are consecutive). The last stage from 438 to 735 °C, with observed weight loss of 12.32%, involves decomposition of two cyanides. The weight increase indicates formation of metal oxide in the last stage, arising from formation of CuO; the final product is a mixture of metallic CuO+Pd (solid residue 41.04%; Calcd 40.25%) for **2** [54,71].

The thermal decomposition of **3** occurs in three steps at 167–259 °C, 259–553 °C, and 553–1214 °C corresponding to release of two *N-bishydeten* and four cyanides. **4** decomposes in three steps with liberation of *N-bishydeten* and four cyanides at 209–294, 294–484, and 484–804 °C.

The DTA profile of **5** shows that the endothermic transition at 125 °C corresponds to a solid–solid transition because no melting was detected. The same behavior was also observed for [Cd(*hydeten*)$_2$Pt(CN)$_4$] [35] and [Cu(*hydeten*)$_2$Pd(CN)$_4$] [38]. The first step which proceeds from 179 to 417 °C with an observed weight loss of 47.78% corresponds to decomposition of two *N-bishydeten* ligands (DTA_{max} 259 °C; Calcd 47.86%). The four cyanides leave upon further heating, and Cd is liberated with a DTG_{max} at 927 °C. The final thermal decomposition product is metallic Pd (solid residue 17.73%; Calcd 17.19%). The thermal stabilities determined from DTG_{max} values of the first decomposition stages change in the order of **1** > **5** > **4** > **3** > **2** and deviate from the Irving-Williams series. The most probable thermal decomposition mechanisms of **1–5** are illustrated in scheme 1.

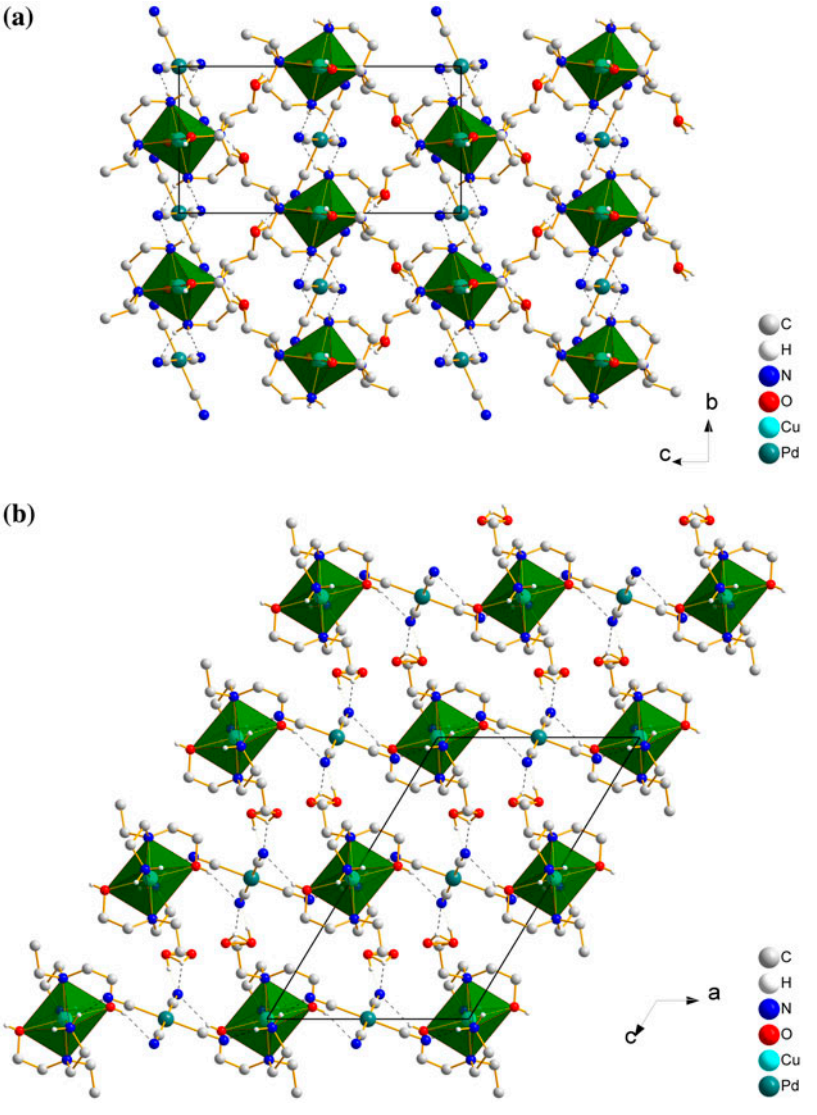

Figure 6. Hydrogen bonds of **3** along (a) the *a* axis and (b) the *b* axis.

3.4. *Catalytic studies*

3.4.1. Heck coupling reaction. The palladium-catalyzed Heck arylation has proven to be one of the most powerful means of forming carbon–carbon bonds in organic synthesis [72] (scheme 2). This efficient metal-catalyzed cross-coupling reaction is regulated by a number of factors such as base, solvent, temperature, and reaction time [73].

The effects of Cs_2CO_3, K_2CO_3, K_3PO_4, and *t*-BuOK on the reaction system were studied; Cs_2CO_3 was effective, whereas the other bases resulted in lower conversions. Solvents such as DMF, DMSO, toluene, dioxane, THF, and CH_3CN had remarkable effects on the

Table 6. Thermoanalytical data for **1–5**.

Complex	Stage	Temperature range (°C)	$DTG_{max.}$ (°C)	ΔH (J/g)	Mass loss, Δm (%) Obs.	Calcd	Liberated group
1	1	238–428	354	17000.26	48.40	47.98	$C_6H_{16}N_2O_2+2CN$
	2	428–733	586	2085.71	11.53	12.47	2CN
2	1	145–206	181	−141.65	2.15	47.43	$C_6H_{16}N_2O_2+2CN$
	2	206–438	317	1426.68	45.07		
	3	438–735	544	−408.90	11.74	12.32	2CN
3	1	167–259	236	3413.26	26.39	25.98	$C_6H_{16}N_2O_2$
	2	259–553	288	−15684.23	32.69	32.69	$C_6H_{16}N_2O_{2+}2CN$
	3	553–1214	1068	63136.08	8.82	9.12	2CN
4	1	209–294	256	197.71	19.72	34.94	$C_6H_{16}N_2O_2$
	2	294–484	311	246.02	14.11		
	3	484–804	497	−259.55	25.02	24.54	4CN
5	1	179–417	259	4346.09	47.78	47.86	$2C_6H_{16}N_2O_2$
	2	417–905	804	827.42	16.48	16.80	4CN
	3	905–1350	927	−42921.42	18.01	18.15	Cd

$[Ni(C_6H_{16}N_2O_2)Pd(CN)_4]$ (**1**) $\xrightarrow[-C_6H_{16}N_2O_2,\ -2CN]{238\text{-}428^oC}$ $[NiPd(CN)_2]$ $\xrightarrow[-2CN]{428\text{-}733^oC}$ PdNi

$[Cu(C_6H_{16}N_2O_2)Pd(CN)_4]$ (**2**) $\xrightarrow[-C_6H_{16}N_2O_2,\ -2CN]{145\text{-}438^oC}$ $[CuPd(CN)_2]$ $\xrightarrow[-2CN]{438\text{-}735^oC}$ CuO+Pd

$[Cu(C_6H_{16}N_2O_2)_2][Pd(CN)_4]$ (**3**) $\xrightarrow[-C_6H_{16}N_2O_2]{167\text{-}259^oC}$ $[Cu(C_6H_{16}N_2O_2)][Pd(CN)_4]$ $\xrightarrow[-C_6H_{16}N_2O_2,\ -2CN]{259\text{-}553^oC}$ $[CuPd(CN)_2]$ $\xrightarrow[-2CN]{553\text{-}1214^oC}$ CuPd

$[Zn(C_6H_{16}N_2O_2)Pd(CN)_4]$ (**4**) $\xrightarrow[-C_6H_{16}N_2O_2]{209\text{-}484^oC}$ $[ZnPd(CN)_4]$ $\xrightarrow[-4CN]{484\text{-}804^oC}$ ZnPd

$[Cd(C_6H_{16}N_2O_2)_2Pd(CN)_4]$ (**5**) $\xrightarrow[-2C_6H_{16}N_2O_2]{179\text{-}417^oC}$ $[CdPd(CN)_4]$ $\xrightarrow[-4\ CN]{417\text{-}905^oC}$ CdPd $\xrightarrow[-Cd]{905\text{-}1350^oC}$ Pd

Scheme 1. Estimated thermal decomposition schemes for **1–5**.

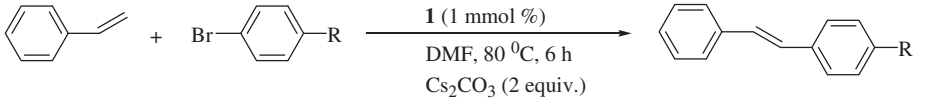

Scheme 2. The Heck reaction of aryl halides with styrene.

coupling reaction. To verify the R group effect in Heck coupling, we investigated a series of reactions involving different R groups (table 7). The optimized conditions of the Pd-catalyzed cross-coupling of 4-bromobenzene with styrene involved performing the reaction in DMF at 80 °C using 1 mol% of **1**, **2,** or **3**. Two equivalents of Cs_2CO_3 were added for **1** and two equivalents of K_2CO_3 were added for **2** and **3**; the best conversions occurred within 6 h for **1** to obtain acceptable yields. The results are summarized in table 7 for these reactions.

Table 7. The Heck coupling reaction of aryl bromides with styrene.

R	Catalyst	Yield[a] (%)
$COCH_3$	**1**	48
CHO	**1**	43
CH_3	**1**	31
H	**1**	35

[a]Reaction conditions: 1.0 mM of R–C_6H_4Br-*p*, 1.5 mM of styrene, 2 mM Cs_2CO_3, 1 mM% Pd complex, DMF (3 mL). Purity of compounds was checked by NMR and yields are based on aryl bromide. All reactions were monitored by GC, 80 °C, 6 h. [b]2 mM K_2CO_3 as a base, 15 h.

Under these reaction conditions, a wide range of aryl bromides bearing electron-donating or electron-withdrawing groups react with styrene, affording the coupled products in yields of 31–48% (table 7, entries 1–4). The activity follows the order R=$COCH_3$ > CHO > H > CH_3. Enhancements in activity, although less significant, were also observed when 4-bromomethylbenzene (entry 3) was used instead of 4-bromoacetophenone (entry 1). Under the optimized conditions, **2** and **3** do not catalyze the Heck reaction; therefore, these complexes are much more stable. Additionally, under these conditions, **1** proved to be a more effective catalyst than **2** and **3**.

3.4.2. Suzuki coupling reaction. The Suzuki reaction is an extremely powerful method for C–C bond formation [27, 74, 75]. To survey the parameters for the Suzuki reaction, we selected Cs_2CO_3, K_2CO_3, and K_3PO_4 as bases and DMF, DMSO, toluene, dioxane, THF, and CH_3CN as solvents. We found that reactions performed with Cs_2CO_3 and **1** in dioxane at 80 °C for 6 h are best. The use of 1% mM **2** and 2 mM K_2CO_3 in dioxane at 80 °C led to the best conversion within 15 h. Table 8 summarizes the results obtained in the presence of **1** and **2** (entries 1–5). The activity follows the order CHO > CH_3 > $COCH_3$ > H. The highest catalytic activity observed was 61% for **1** and 75% for **2** (table 8). The scope of the cross-coupling reaction with respect to aryl bromide was also investigated; **2** is an effective complex for coupling unactivated, activated, and deactivated bromides (scheme 3).

3.5. *EPR studies*

We were unable to obtain EPR spectra of **1** because of the short relaxation times of Ni^{II} in an octahedral environment at room temperature.

Table 8. The Suzuki coupling of aryl bromides with phenylboronic acid.

R	Catalyst	Yield[a] (%)
$COCH_3$	**1**	49
CHO	**1**	61
CH_3	**1**	56
H	**1**	39
$COCH_3$	**2**	75[b]

[a]Reaction conditions: 1.0 mM of R–C_6H_4Br-*p*, 1.5 mM of phenylboronic acid, 2 mM Cs_2CO_3, 1 mM% Pd complex, dioxane (3 mL). Purity of compounds was checked by NMR and yields are based on aryl bromide. All reactions were monitored by GC, 80 °C, 6 h. [b]2 mM K_2CO_3 as a base, 15 h.

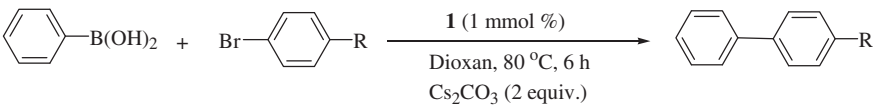

Scheme 3. The Suzuki coupling of aryl bromides with phenylboronic acid.

The room temperature powder EPR spectra of **2** and **3** are shown in Supplementary material. Hyperfine splitting could not be resolved because of line broadening originating from spin-exchange and spin-orbit interactions that result from excess spin concentration. The $g_{\parallel}$ and $g_{\perp}$ values extracted from the powder spectra are: $g_{\parallel}=2.224$, $g_{\perp}=2.060$ for **2** and $g_{\parallel}=2.252$, $g_{\perp}=2.063$ for **3**. These g parameters indicate that the paramagnetic center for each powder sample is axially symmetric, attributed to a Cu^{II} ($S=1/2$, $I=3/2$). Because $g_{\parallel}>g_{\perp}>g_e$ (free electron g value, $g_e=2.0023$), it can be concluded that Cu^{II} is in tetragonally distorted octahedral sites (D_{4h}) elongated along the z-axis, and the ground state of the paramagnetic electron is $d_{x^2-y^2}$ ($^2B_{1g}$ state) [76–79].

The Pd^{II} ions in these complexes have square-planar coordination geometries and are low spin (S=0) and thus, diamagnetic. For this reason, no EPR signal for Pd ions is observed.

3.6. *Magnetic properties*

The magnetic susceptibility of **1–3** was obtained from 10 to 300 K. The temperature dependence of the molar magnetic susceptibilities (χ_m) and $\chi_m T$ are shown in figures 7–9 for these complexes. The variable temperature dependence of χ_m for **1** and **2** was fitted using the relation $C/(T-\theta)$, where C is the Curie constant and θ is the Weiss constant [80]. From this fitting process, the relationships $C=1.2006\pm0.0002$ emuK/mol.Oe and $\theta=-0.968\pm0.002$ K were determined for **1** and $C=0.459\pm0.00004$ emuK/mol.Oe and

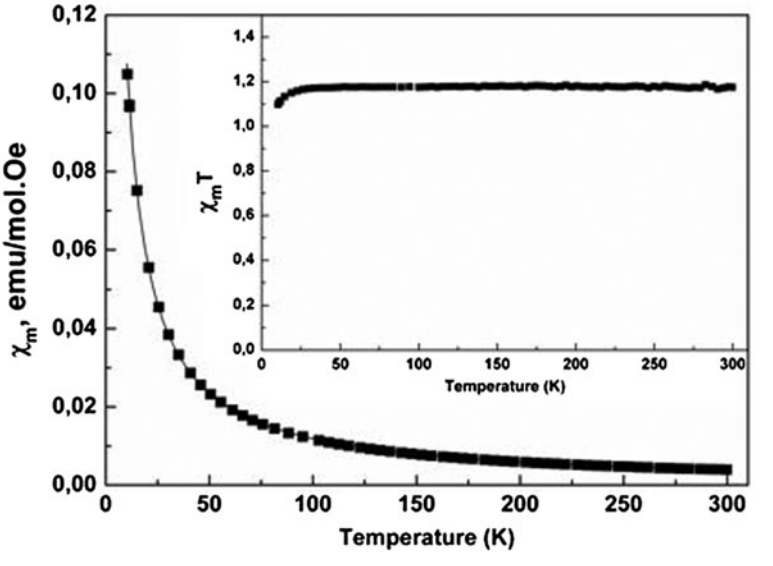

Figure 7. The temperature dependence of the molar magnetic susceptibility χ_m for **1**. Solid line represents a fit by the Curie–Weiss law. Inset: the temperature dependence of χ_mT.

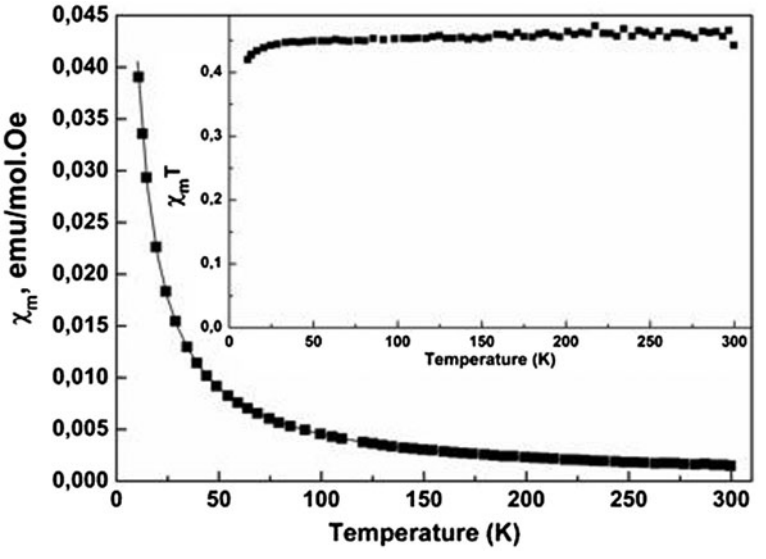

Figure 8. The temperature dependence of the molar magnetic susceptibility χ_m for **2**. Solid line represents a fit by the Curie–Weiss law. Inset: the temperature dependence of $\chi_m T$.

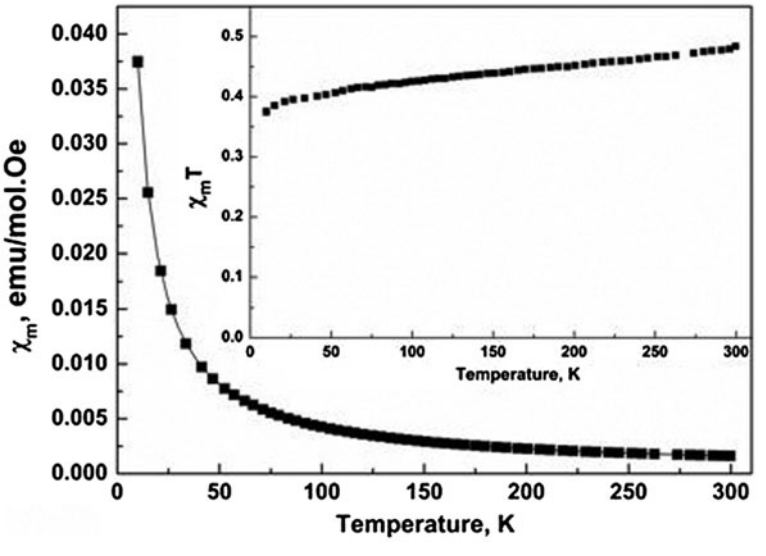

Figure 9. The temperature dependence of the molar magnetic susceptibility χ_m for **3**. Solid line represents a fit by the Curie–Weiss law. Inset: the temperature dependence of $\chi_m T$.

$\theta = -1.022 \pm 0.001$ K for **2**. The effective magnetic moment, μ_{eff}, was calculated to be 3.10 for **1** and 1.917 for **2** using the relation $\mu_{eff} = 2.83(C)^{1/2}$ and is expressed in Bohr magnetons (μ_B). The values of μ_{eff} for **1** and **2** are greater than the spin-only value due to mixing of some spin-orbital angular momentum from excited states via spin-orbit coupling [81].

For **3**, the temperature dependence of χ_m was fitted using the relation $\alpha + C/(T-\theta)$, where α is the temperature-independent susceptibility [80]. Based on this fitting, the relationships $C = 0.39778 \pm 0.00005$ emuK/mol.Oe, $\alpha = 0.00029 \pm 0.0000005$ emu/mol.Oe, and $\theta = -0.672 \pm 0.001$ K were determined. Thus, there is temperature-independent paramagnetism (α), originating from coupling between the ground state and the excited states due to orbital moments of the d electrons or from the presence of conducting electrons. The effective magnetic moment for **3**, μ_{eff}, was calculated to be 1.783 in Bohr magnetons (μ_B).

Below 10 K, there may be a slight antiferromagnetic interaction in **1–3**, as observed from the insets of figures 7–9. The insets also measure effective magnetic moment ($\mu_{eff} = 2.83\ \sqrt{\chi_m T}$). This magnetic interaction might be between and within the chains involving CN^- bridges and hydrogen bonds.

4. Conclusion

Five heterometallic cyanide complexes containing tetracyanidopalladate and *N-bishydeten* have been prepared and two of these complexes were characterized using X-ray crystallography. Different assembly chemistry of $[Cu(N\text{-}bishydeten)_n]^{+2}$ ($n = 1$ or 2) with the $[Pd(CN)_4]^{2-}$ complex anion is observed. *N-bishydeten* is a tetradentate ligand in **2** and tridentate in **3** with NN′O donors.

The N–H···(N≡C) interactions are shorter than the upper limit for an N···N distance. IR spectra of **1–5** were recorded and confirmed the presence of all functional groups in the complexes. According to DTG_{max} values, the first decomposition stage changes **1** > **5** > **4** > **3** > **2** and deviates from the Irving-Williams series.

1–3 were tested as catalysts, and **1** proved to be more effective in Heck coupling and **2** is an effective complex for coupling unactivated, activated, and deactivated bromides in a Suzuki reaction.

Below 10 K, there may be a slight antiferromagnetic interaction in the structures of **1–3**. This magnetic interaction might be between and within chains involving CN^- bridges and hydrogen bonds.

Acknowledgments

The authors thank the Scientific and Technical Research Council of Turkey (TUBİTAK, Grant TBAG-104T205) and the Gaziosmanpaşa University Research Foundation (Grant 2010/110) for financial support.

References

[1] M. Pilkington, S. Decurtins. In *Comprehensive Coordination Chemistry II*, A.M. Cleverty, T.J. Meyer (Eds), Vol. 7, pp. 177–179, Elsevier, Amsterdam (2003).
[2] J. Černák, M. Orendáč, I. Potočňák, J. Chomič, A. Orendáčová, J. Skoršepa, A. Feher. *Coord. Chem. Rev.*, **224**, 51 (2002).
[3] G.M. Davies, S.J.A. Pope, H. Adams, S. Faulkner, M.D. Ward. *Inorg. Chem.*, **44**, 4656 (2005).
[4] J.M. Herrera, S.J.A. Pope, H. Adams, S. Faulkner, M.D. Ward. *Inorg. Chem.*, **45**, 3895 (2006).
[5] D.J. Darensbourg, A.L. Phelps. *Inorg. Chim. Acta*, **357**, 1603 (2004).
[6] R. Brahmi, C. Kappenstein, J. Černák, D. Duprez, A. Sadel. *J. Phys. Chem.*, **96**, 487 (1999).
[7] D. William, J. Kouvetakis, M. O'Keefe. *Inorg. Chem.*, **37**, 4617 (1998).

[8] M.P. Shores, L.G. Beauvais, J.R. Long. *J. Am. Chem. Soc.*, **121**, 775 (1999).
[9] M.P. Shores, L.G. Beauvais, J.R. Long. *Inorg. Chem.*, **38**, 1648 (1999).
[10] M.V. Bennett, L.G. Beauvais, M.P. Shores, J.R. Long. *J. Am. Chem. Soc.*, **123**, 8022 (2001).
[11] M. Kämper, M. Wagner, A. Weiss. *Angew. Chem. Int. Ed.*, **91**, 517 (1979).
[12] T. Niu, A.J. Jacobson. *Inorg. Chem.*, **38**, 5346 (1999).
[13] K.K. Klausmeyer, T.B. Rauchfuss, S.R. Wilson. *Angew. Chem. Int. Ed.*, **37**, 1694 (1998).
[14] A.M.A. Ibrahim. *Polyhedron*, **18**, 2711 (1999).
[15] L. Ouyang, P.M. Aguiar, R.J. Batchelor, S. Kroeker, D.B. Leznoff. *Chem. Commun.*, **7**, 744 (2006).
[16] L. Jiang, X.L. Feng, T.B. Lu, S. Gao. *Inorg. Chem.*, **45**, 5018 (2006).
[17] M. Atanasov, P. Comba, S. Förster, G. Linti, T. Malcherek, R. Miletich, A.I. Prikhodko, H. Wadepohl. *Inorg. Chem.*, **45**, 7722 (2006).
[18] R. Lescoüezec, L.M. Tomaa, J. Vaissermann, M. Verdaguer, F.S. Delgado, C. Ruiz-Pérez, F. Lloret, M. Julve. *Coord. Chem. Rev.*, **249**, 2691 (2005).
[19] S. Tanase, J. Reedijk. *Coord. Chem. Rev.*, **250**, 2501 (2006).
[20] H.J. Choi, J.J. Sokol, J.R. Long. *Inorg. Chem.*, **43**, 1606 (2004).
[21] I. Muga, J.M. Gutiérrez-Zorrilla, P. Vitoria, P. Román, F. Lloret. *Polyhedron*, **21**, 2631 (2002).
[22] D. Steinborn. *Grundlagen der metallorganischen Komplexkatalyse* [Basics of Organometallic Complex Catalysis], Teubner, Wiesbaden (2007).
[23] M. Beller, C. Bolm, *Transition Metals for Organic Synthesis*, Vol.1, 2nd Edn, Wiley-VCH, Weinheim (2004).
[24] B. Cornils, W.A. Herrmann. *Applied Homogeneous Catalysis with Organometallic Compounds*, Wiley-VCH, Weinheim (1996).
[25] N.T.S. Phan, M.V.D. Sluys, C.W. Jones. *Adv. Synth. Catal.*, **348**, 609 (2006).
[26] F. Diederich, P.J. Stang. *Metal-catalyzed Cross-coupling Reactions*, 2nd Edn, Wiley-VCH, Weinheim (2004).
[27] N. Miyaura, A. Suzuki. *Chem. Rev.*, **95**, 2457 (1995).
[28] Y. Tsuji, T. Fujihara. *Inorg. Chem.*, **46**, 1895 (2007).
[29] S. Kotha, K. Lahiri. *Eur. J. Org. Chem.*, **1221**, (2007).
[30] M. Weck, C.W. Jones. *Inorg. Chem.*, **46**, 1865 (2007).
[31] V.P.W. Böhm. Catalytic activation of aryl chlorides in Heck-type reactions. PhD thesis, TU-München (2000).
[32] D. Astruc. *Inorg. Chem.*, **46**, 1884 (2007).
[33] S. Körbe. Formation of bicyclic and tricyclic systems by a domino process of palladium-catalyzed cyclization and Diels-Alder reaction. PhD thesis, Georg-August-Universität Göttingen (2001).
[34] W.A. Herrmann, C. Broßmer, K. Öfele, M. Beller, H. Fischer. *J. Organomet. Chem.*, **491**, C1 (1995).
[35] A. Karadağ, İ. Önal, A. Şenocak, İ. Uçar, A. Bulut, O. Büyükgüngör. *Polyhedron*, **27**, 223 (2008).
[36] A. Karadağ, Ş.A. Korkmaz, Ö. Andaç, Y. Yerli, Y. Topçu. *J. Coord. Chem.*, **65**, 1685 (2012).
[37] B. Song, J. Reuber, C. Ochs, F.E. Hahn, T. Lügger, C. Orvig. *Inorg. Chem.*, **40**, 1527 (2001).
[38] A. Karadağ. *Z. Kristallogr.*, **222**, 39 (2007).
[39] A. Karadağ, A. Bulut, A. Şenocak, İ. Uçar, O. Büyükgüngör. *J. Coord. Chem.*, **60**, 2035 (2007).
[40] A. Karadağ, A. Şenocak, Y. Yerli, E. Şahin, R. Topkaya. *J. Inorg. Organomet. Polym.*, **22**, 369 (2012).
[41] A. Şenocak, A. Karadağ, Y. Yerli, N. Gürbüz, İ. Özdemir, E. Şahin. *Polyhedron*, **49**, 50 (2013).
[42] Rigaku, Rigaku American Corporation 9009 New Trails Drive, Crystal-clear *(Version 1.3.6)*, The Woodlands, TX, USA (2005).
[43] G.M. Sheldrick. *Acta Crystallogr.*, **A64**, 112 (2008).
[44] Stoe & Cie. *X-Area (Version 1.18) and X-Red32 (Version 1.04)*, Stoe & Cie, Darmstadt, Germany (2002).
[45] L.J. Farrugia. *J. Appl. Crystallogr.*, **30**, 565 (1997).
[46] L.J. Farrugia. *J. Appl. Crystallogr.*, **32**, 837 (1999).
[47] K. Brandenburg. *DIAMOND (Release 2.1e) Crystal Impact GbR*, Bonn, Germany (2000).
[48] K. Nakamoto, *Infrared and Raman Spectra of Inorganic and Coordination Compounds*, 4th Edn, pp. 272–273, Wiley-Interscience, New York (1978).
[49] S.C. Manna, J. Ribas, E. Zangrando, N.R. Chaudhuri. *Polyhedron*, **26**, 3189 (2007).
[50] A. Şenocak, Supervisor: A. Karadağ. Investigation of Synthesis, Structure and Properties of New Cyano-Bridged Polymeric Transition Metal Complexes. PhD thesis, University of Gaziosmanpaşa (2010).
[51] J. Černák, J. Skoršepa, K.A. Abboud, M.W. Meisel, M. Orendáč, A. Orendáčová, A. Feher. *Inorg. Chim. Acta*, **326**, 3 (2001).
[52] A.O. Legendre, A.E. Mauro, M.A.R. Oliveira, M.T.P. Gambardella. *Inorg. Chem. Commun.*, **11**, 896 (2008).
[53] J. Kuchár, J. Černák, K.A. Abboud. *Acta Crystallogr.*, **C60**, m492 (2004).
[54] T. Akitsu, Y. Einaga. *Inorg. Chim. Acta*, **361**, 36 (2008).
[55] A. Şenocak, A. Karadağ, Y. Yerli, Ö. Andaç, E. Şahin. *J. Inorg. Organomet. Polym.*, **20**, 628 (2010).
[56] A. Karadağ, A. Şenocak, İ. Önal, Y. Yerli, E. Şahin, A.C. Başaran. *Inorg. Chim. Acta*, **362**, 2299 (2009).
[57] H. Zhang, J. Cai, X. Feng, H. Sang, J. Liu, X. Li, L. Ji. *Polyhedron*, **21**, 721 (2002).
[58] M. Ruegg, A. Ludi. *Theor. Chim. Acta*, **20**, 193 (1971).
[59] A. Karadağ, H. Paşaoğlu, G. Kaştaş, O. Büyükgüngör. *Acta Crystallogr.*, **C60**, m581 (2004).

[60] A. Karadağ, TUBITAK (Scientific and Technical Research Council of TURKIYE), Grant No: 104T205 (2010).
[61] S. Perruchas, K. Boubekeur, P. Molinié. *Polyhedron*, **24**, 1555 (2005).
[62] D. Visinescu, J.-P. Sutter, C. Duhayon, A.M. Madalan, B. Jurca, M. Andruh. *J. Coord. Chem.*, **64**, 93 (2011).
[63] S.J. Ludy, C.P. Landee, M.M. Turnbull, J.L. Wikaira. *J. Coord. Chem.*, **64**, 134 (2011).
[64] S.R. Chowdhury, M.D. Selim, S. Chatterjee, S. Igarashi, Y. Yukawa, K.K. Mukherjea. *J. Coord. Chem.*, **65**, 3469 (2012).
[65] J. Xia, T.-T. Li, X.-Q. Zhao, J.-F. Wei. *J. Coord. Chem.*, **66**, 539 (2013).
[66] J. Černák, J. Chomič, I. Potočňák. *J. Therm. Anal.*, **35**, 2265 (1989).
[67] J. Černák, I. Potočňák, J. Chomič. *J. Therm. Anal.*, **39**, 849 (1993).
[68] J. Černák, J. Skoršepa, J. Chomič, I. Potočňák, J. Hoppan. *J. Therm. Anal.*, **41**, 91 (1994).
[69] V.T. Yılmaz, A. Karadağ. *Thermochim. Acta*, **348**, 121 (2000).
[70] F. Yakuphanoğlu, A. Karadağ, M. Şekerci. *J. Therm. Anal.*, **86**, 727 (2006).
[71] A. Şenocak, A. Karadağ, E. Şahin, Y. Yerli. *J. Inorg. Organomet. Polym.*, **21**, 438 (2011).
[72] A.E. Wang, J.H. Xie, L.X. Wang, Q.L. Zhou. *Tetrahedron*, **61**, 259 (2005).
[73] J.P. Corbet, G. Mignani. *Chem. Rev.*, **106**, 2651 (2006).
[74] S.P. Stanforth. *Tetrahedron*, **54**, 263 (1998).
[75] A. Suzuki. *J. Organomet. Chem.*, **576**, 147 (1999).
[76] R.J. Dudley, B.J. Hathaway. *J. Chem. Soc.*, 2799 (1970).
[77] E.D. Mauro, S.M. Domiciano. *J. Phys. Chem. Solids*, **60**, 1849 (1999).
[78] Y. Yerli, S. Kazan, O. Yalçın, B. Aktas. *Spectrochim. Acta, Part A*, **64**, 642 (2006).
[79] Y. Yerli, F. Köksal, A. Karadag. *Solid State Sci.*, **5**, 1319 (2003).
[80] J.J. Earney, C.P.B. Finn, B.M. Najafabadi. *J. Phys. C: Solid State Phys.*, **4**, 1013 (1971).
[81] B.J. Hathaway, D.E. Billing. *Coord. Chem. Rev.*, **5**, 143 (1970).